

Reconstruction of Multivariate Sparse Signals from Mismatched Samples

Taulant Koka, Michael Muma and Benjamín Béjar Haro

Abstract—Erroneous correspondences between samples and their respective channel or target commonly arise in several real-world applications. For instance, whole-brain calcium imaging of freely moving organisms, multiple target tracking or multi-person contactless vital sign monitoring may be severely affected by mismatched sample-channel assignments. To systematically address this fundamental problem, we pose it as a signal reconstruction problem where we have lost correspondences between the samples and their respective channels. We show that under the assumption that the signals of interest admit a sparse representation over an overcomplete dictionary, unique signal recovery is possible. Our derivations reveal that the problem is equivalent to a structured unlabeled sensing problem without precise knowledge of the sensing matrix. Unfortunately, existing methods are neither robust to errors in the regressors nor do they exploit the structure of the problem. Therefore, we propose a novel robust two-step approach for the reconstruction of shuffled sparse signals. The performance and robustness of the proposed approach is illustrated in an application of whole-brain calcium imaging in computational neuroscience. The proposed framework can be generalized to sparse signal representations other than the ones considered in this work to be applied in a variety of real-world problems with imprecise measurement or channel assignment.

Index Terms—Unlabeled Sensing, Sparsity, Sampling.

I. INTRODUCTION

THE problem of reconstructing a signal without precise knowledge about the sample locations has recently received considerable attention from the research community. In a discrete setting, such a problem is usually referred to as *unlabeled sensing* or *shuffled linear regression* [1]. In shuffled linear regression, the sensing matrix is assumed to be known and the goal is to recover the right ordering (permutation matrix) together with the regression coefficients that generated the observations. Here, we consider a related problem where the sensing matrix is not precisely known *a priori*, and where the shuffling of samples does not happen within the signal but rather across multiple channels of a multivariate signal (see Figs. 1 and 2). Our setting is thus more general in the sense that the exact sensing matrix is not precisely known *a priori*. At the same time, it also adds more structure due to swapping of samples across channels only and, to the best of our knowledge, our problem setup has not been considered previously in the literature. Such a setup broadly applies to

situations where some quantity of interest is measured from multiple moving targets that may be difficult to tell apart due to partial occlusions, crossings or measurement noise (Fig. 1 (a)). For instance, entomological radar for observing insect flight and migration [2], fluorescence microscopy of moving cell cultures [3], contactless vital sign monitoring of groups of people or animals [4], [5], multiple target tracking [6], [7] or whole-brain calcium imaging of freely moving organisms such as *zebrafish* or *C. elegans* [8] constitute some paradigmatic examples (Fig. 1 (b)). Of course, without any prior knowledge about the signals of interest the problem is hopeless. In our case, we rely on the assumption that the signals of interest (each of the channels) admit a sparse representation in an overcomplete dictionary with possibly infinitely many elements. This allows us to first retrieve the support of the signal and estimate the sensing matrix that is subsequently used to solve the sample assignment and signal reconstruction problems.

Main Contributions: We address the problem of multi-channel signal reconstruction from corrupted measurements without precise channel correspondences. Our major original contributions are as follows: (i) We formalize the signal estimation problem assuming that the signals can be sparsely represented on a dictionary over the continuum. (ii) We show that such representation allows the estimation of the true signal support and conditions on the uniqueness of the solution are established by relating the problem to that of unlabeled sensing. (iii) We propose a two-step approach for signal estimation that relies on an iterative robust regression procedure to determine the correct sample-channel assignment and regression coefficients. A python implementation will be made available on the authors github page. (iv) We demonstrate and benchmark the performance of the proposed methodology against competing methods in Monte Carlo experiments related to whole-brain calcium imaging in neuroscience.

II. SHUFFLED MULTI-CHANNEL SPARSE SIGNALS

We start by introducing the considered class of signals of interest and the problem setup. In our notation, we use capital letters to denote frequency domain representations and bold-faced letters to denote vectors and matrices. For the sake of argument and evaluation, we focus our attention on the two-channel case. The results for more than two channels are also stated but the technical derivation is deferred to the appendix.

A. Sparse Signal Model

Let $\mathbf{x}_m = (x_{m,0}, \dots, x_{m,N-1})^\top$, $m = 1, \dots, M$ be the sampled signal of the m th channel and let

Taulant Koka and Michael Muma are with the Robust Data Science Group at Technische Universität Darmstadt, Germany (e-mail: taulant.koka@tu-darmstadt.de; michael.muma@tu-darmstadt.de).

Benjamín Béjar Haro is with the Swiss Data Science Center at the Paul Scherrer Institute, Switzerland (e-mail: benjamin.bejar@psi.ch).

The work of the first and second author has been funded by the ERC Starting Grant ScReeningData under grant number 101042407.

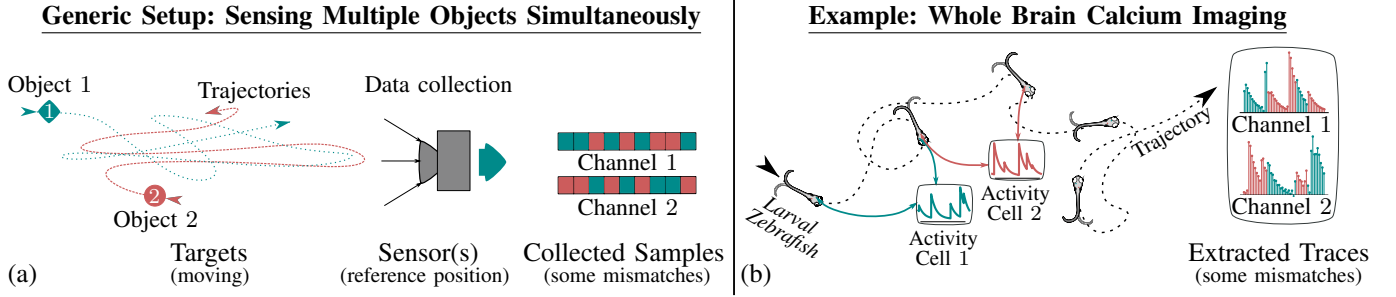


Fig. 1. **Settings without precise sample-channel assignments:** (a) Illustration of the generic setting in which acquired samples of some multivariate quantity of interest (Object 1 and 2) may be shuffled (Channel 1 and 2) due to crossings, occlusions, or measurement noise. (b) Real-world application example in whole-brain calcium imaging. Traces of neuronal activity may be shuffled, due to wrongly annotated neurons.

$[\text{DFT}_N(\cdot)]_\ell$, $\ell = 0, \dots, N - 1$ denote the ℓ th element of the N -point discrete Fourier transform (DFT) of a discrete vector signal. We assume that the discrete signal \mathbf{x}_m has a frequency domain representation given by a mixture of K_m complex exponentials:

$$X_{m,\ell} := [\text{DFT}_N(\mathbf{x}_m)]_\ell = \sum_{k=0}^{K_m-1} a_{m,k} e^{-j2\pi\ell t_{m,k}}, \quad (1)$$

$$\ell = 0, \dots, N - 1, \quad t_{m,k} \in [0, 1), \quad a_{m,k} \in \mathbb{C}.$$

Remark 1. Note that since (1) represents a pointwise regular sampling of the spectrum of a signal that is a mixture of complex exponentials, it has a sparse representation in the time domain (stream of Dirac delta functions) at locations $\{t_{m,k}\}_{k=0}^{K_m-1}$ and with corresponding amplitudes $\{a_{m,k}\}_{k=0}^{K_m-1}$.

Remark 2. Note also that our setup would apply to continuous-time signals with an appropriate sampling setup as in Fig. 2 (a) (e.g., signals with Finite Rate of Innovation (FRI signals) [9]) as long as the DFT of the samples satisfies (1).

Our case of study concerns the reconstruction of signals with DFT of the form in (1) when there is no precise assignment between channels and available measurements, i.e., the signals \mathbf{x}_m have been shuffled across channels. More precisely, let \mathbf{y}_m be the observed signal in the m th channel. We say that the measurements $\mathbf{Y} = (\mathbf{y}_1, \mathbf{y}_2, \dots, \mathbf{y}_M)$ are shuffled multi-channel measurements of the corresponding signals $\mathbf{X} = (\mathbf{x}_1, \mathbf{x}_2, \dots, \mathbf{x}_M)$ if each row of \mathbf{Y} equals the corresponding row in \mathbf{X} up to a permutation of the values.

An illustration of the shuffling process is exemplified in Fig. 2 (a), where a full sampling setup is displayed. The acquisition of two discrete measurement vectors $\mathbf{y}_1, \mathbf{y}_2$ is broken down into two parts: (i) one-dimensional continuous-time signals $z_m(t)$, $m = 1, 2$ are filtered with a sampling kernel $\varphi^*(-t/T_s)$ and sampled with sampling period $T_s = 1/N$ at the discrete locations nT_s , $n = 0, \dots, N - 1$, resulting in discrete time series $x_{1,n}, x_{2,n}$, and (ii) the samples $x_{1,n}, x_{2,n}$ are permuted at some discrete time points, resulting in the sequences $y_{1,n}, y_{2,n}$. The shuffling process is also illustrated in Fig. 2 (b) for $M = 5$ channels (represented by colored columns) showing the equivalence

to permuting the elements of individual rows in the matrix \mathbf{X} .

Let us now turn our attention to the two-channel scenario and relate the observed and original signals via a permutation matrix.

Definition 1. (Permutation Matrix) A square matrix $\mathbf{\Pi}$ is a permutation matrix if it corresponds to a reordering of the columns (or rows) of the identity matrix, i.e., $\mathbf{\Pi}\mathbf{\Pi}^\top = \mathbf{\Pi}^\top\mathbf{\Pi} = \mathbf{I}$, $[\mathbf{\Pi}]_{ij} \in \{0, 1\}$. Thus, a permutation matrix has exactly a single '1' per row and column.

In order to show the relation, let us introduce the binary vector $\mathbf{q} \in \{0, 1\}^N$ as an indicator variable to denote whether or not the measurements have been shuffled between the two channels. If we let $\mathbf{Q} = \text{diag}(\mathbf{q})$ then we can express the multi-channel shuffled measurement vectors $\mathbf{y}_1, \mathbf{y}_2$ as

$$\begin{aligned} \mathbf{y}_1 &= \mathbf{Q}\mathbf{x}_1 + (\mathbf{I} - \mathbf{Q})\mathbf{x}_2 \\ \mathbf{y}_2 &= (\mathbf{I} - \mathbf{Q})\mathbf{x}_1 + \mathbf{Q}\mathbf{x}_2 \end{aligned} \quad (2)$$

The above system of equations can be rewritten in block matrix notation as

$$\underbrace{\begin{pmatrix} \mathbf{y}_1 \\ \mathbf{y}_2 \end{pmatrix}}_{:=\mathbf{y}} = \underbrace{\begin{pmatrix} \mathbf{Q} & \mathbf{I} - \mathbf{Q} \\ \mathbf{I} - \mathbf{Q} & \mathbf{Q} \end{pmatrix}}_{:=\mathbf{\Pi}_q} \underbrace{\begin{pmatrix} \mathbf{x}_1 \\ \mathbf{x}_2 \end{pmatrix}}_{:=\mathbf{x}}. \quad (3)$$

In this notation, it is clear from Definition 1 that the shuffling of the two signals corresponds to the matrix-vector product of an unknown structured permutation matrix $\mathbf{\Pi}_q$ and an unknown stacked vector \mathbf{x} . In general, trying to solve (3) for $\mathbf{\Pi}_q$ and/or \mathbf{x} is an ill-posed problem if no further assumptions are made. However, for sparse signals of the form of (1) we shall derive conditions on the number of samples for which the decomposition in (3) is unique.

B. Unlabeled Sensing and Uniqueness

Under the assumption that the true signals \mathbf{x}_m satisfy (1), it is possible to estimate the parameters of the signals $\Theta_m = (\{t_{m,k}, a_{m,k}\}_{k=0}^{K_m-1})$ provided the number of measurements N is sufficiently large. In particular, it is well-known that for a uniformly sampled mixture of K distinct complex exponentials as in (1), a number of $N = 2K$ samples uniquely determines the parameters of the mixture by using line spectral estimation methods [10]. In our case, we do not have access to

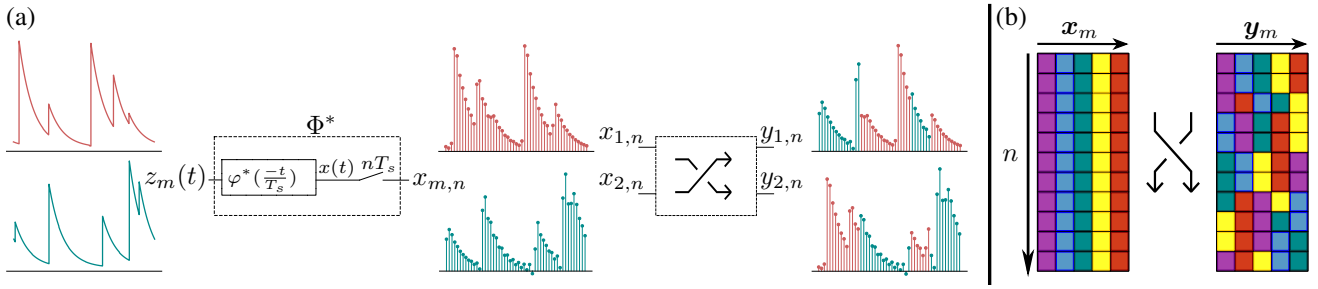


Fig. 2. **Shuffled sampling:** (a) The measurements \mathbf{y}_m are modeled as a shuffling of the samples in the unknown true signals \mathbf{x}_m at each sampling point n . (b) If the individual signals \mathbf{x}_m represent the columns in a data matrix the shuffling corresponds to a permutation of each individual row.

such measurements due to the shuffling of the temporal signals \mathbf{x}_m . Instead, the special structure of (3) allows us to look at the addition of the measured vectors since this quantity is invariant w.r.t. the permutation of the samples across channels. For the two-channel case, this amounts to

$$\begin{aligned} x_{1,n} + x_{2,n} &= x_{2,n} + x_{1,n} \\ \implies \mathbf{x}_\Sigma &:= \mathbf{x}_1 + \mathbf{x}_2 = \mathbf{y}_1 + \mathbf{y}_2 =: \mathbf{y}_\Sigma. \end{aligned} \quad (4)$$

Based on the above observation, $[\text{DFT}_N(\mathbf{x}_\Sigma)]_\ell$ is again a mixture of complex exponentials as defined in (1). Let us now denote $\Theta_\Sigma = (\{a_{\Sigma,k}, t_{\Sigma,k}\}_{k=0}^{K_\Sigma-1}, t_{\Sigma,k} \in [0, 1), a_{\Sigma,k} \in \mathbb{C})$ the parameters of the mixture, where K_Σ is the number of distinct locations $t_{\Sigma,k}$ in the mixture with corresponding amplitudes $a_{\Sigma,k}$. Therefore, if the number of samples $N \geq 2K_\Sigma$, it is possible to retrieve the parameters Θ_Σ (and hence a basis for the measured signals) by using line spectral estimation methods such as Prony's method [11]. With the recovered parameters, we can now express the sum of samples given by (4) as $\mathbf{x}_\Sigma = \mathbf{W}\mathbf{V}_\Sigma\mathbf{a}_\Sigma$, where \mathbf{W} is the inverse discrete Fourier transform (IDFT) matrix, \mathbf{V}_Σ is a Vandermonde matrix constructed from the locations $t_{\Sigma,k}$ of the mixture signal (i.e., $[\mathbf{V}_\Sigma]_{\ell,k} = v_k^\ell$ with $v_k = e^{-j2\pi t_{\Sigma,k}}$), and where \mathbf{a}_Σ is a vector containing the corresponding amplitudes. By defining $\mathbf{U} := \mathbf{W}\mathbf{V}_\Sigma$, we can then express the individual channels as a linear system of equations, i.e.,

$$\begin{pmatrix} \mathbf{x}_1 \\ \mathbf{x}_2 \end{pmatrix} = \begin{pmatrix} \mathbf{U} & \\ & \mathbf{U} \end{pmatrix} \begin{pmatrix} \beta_1 \\ \beta_2 \end{pmatrix}, \quad \beta_1, \beta_2 \in \mathbb{R}^{K_\Sigma}, \quad (5)$$

where, in general, β_1 and β_2 are unknown. Note that \mathbf{U} has full column rank since the $t_{\Sigma,k}$ of \mathbf{x}_Σ are distinct. Since $\mathbf{x}_1, \mathbf{x}_2 \in \mathcal{R}(\mathbf{U})$, i.e., \mathbf{x}_1 and \mathbf{x}_2 lie in the range of \mathbf{U} , it follows that (5) has a unique solution (assuming $\mathbf{x}_1, \mathbf{x}_2$ are known). In fact, the nonzero elements in β_1 and β_2 correspond, respectively, to the amplitudes \mathbf{a}_1 and \mathbf{a}_2 of the individual signals. Thus, the nonzero elements of $\beta := (\beta_1^\top, \beta_2^\top)^\top$ determine which Diracs should be included in the respective signals and what the corresponding amplitudes are. Combining (3) and (5) yields:

$$\underbrace{\begin{pmatrix} \mathbf{y}_1 \\ \mathbf{y}_2 \end{pmatrix}}_{:=\mathbf{y}} = \underbrace{\begin{pmatrix} \mathbf{Q} & \mathbf{I} - \mathbf{Q} \\ \mathbf{I} - \mathbf{Q} & \mathbf{Q} \end{pmatrix}}_{:=\mathbf{\Pi}_q} \underbrace{\begin{pmatrix} \mathbf{U} \\ \mathbf{U} \end{pmatrix}}_{:=\mathbf{A}} \underbrace{\begin{pmatrix} \beta_1 \\ \beta_2 \end{pmatrix}}_{:=\beta}, \quad (6)$$

where the matrix \mathbf{A} is block diagonal with diagonal elements \mathbf{U} and thus, has full column rank as long as \mathbf{U} has full column rank. For an unknown permutation matrix $\mathbf{\Pi}_q$ and unknown

regression coefficients β , (6) corresponds to a structured unlabeled sensing formulation. From [1], [12], [13], it is known that the shuffled linear regression problem admits a unique solution under certain conditions. Here, we will restate Corollary 1 of [12], which is relevant for our purpose, in a slightly reformulated manner.

Corollary 1 (Dokmanić, 2019 [12]). *If $\mathbb{P} \subset \mathbb{R}^{N \times N}$ is the set of all $N!$ permutation matrices of N elements, then any β can be uniquely recovered from measurements $\mathbf{y} = \mathbf{\Pi}\mathbf{A}\beta$, where both $\mathbf{\Pi} \in \mathbb{P}$ and $\beta \in \mathbb{C}^m$ are unknown, for almost all matrices $\mathbf{A} \in \mathbb{C}^{N \times K}$ (that is, for \mathbf{A} with full column rank) with $N \geq 2K$. Conversely, if $N < 2K$ then for almost all \mathbf{A} there exist $\beta \neq \zeta$ and permutations $\mathbf{\Pi}_1 \neq \mathbf{\Pi}_2$ such that $\mathbf{\Pi}_1\mathbf{A}\beta = \mathbf{\Pi}_2\mathbf{A}\zeta$.*

Corollary 1 states that the regression coefficients in (6) are uniquely determined as long as $N \geq 2K_\Sigma$ and \mathbf{A} has full column rank and thus we have just shown that in the case of two shuffled signals with DFT as in (1), the original signals can be uniquely recovered provided that $N \geq 2K_\Sigma$.

We have just provided a constructive proof for the uniqueness of the solution in the two-channel case. The result generalizes to more than two signals and the proof parallels the derivations in this section. We state here our main (general) result, for a formal proof we refer the reader to Appendix A.

Theorem 1. *Let $\mathbf{y}_1, \mathbf{y}_2, \dots, \mathbf{y}_M \in \mathbb{R}^N$ be multi-channel shuffled measurement vectors of some unknown noiseless sample vectors $\mathbf{x}_1, \mathbf{x}_2, \dots, \mathbf{x}_M \in \mathbb{R}^N$ whose DFT consist of uniformly sampled mixtures of complex exponentials of the form*

$$X_{m,\ell} = \sum_{k=0}^{K_m-1} a_{m,k} e^{-j2\pi\ell t_{m,k}} \quad (7)$$

with $\ell = 0, \dots, N-1$, $t_{m,k} \in [0, 1)$, and that are fully specified by the set of parameters $\{(a_{m,k}, t_{m,k})_{k=0}^{K_m-1}\}$, $m = 1, \dots, M$, where K_m is the number of distinct locations $t_{m,k}$ in the m th signal. Furthermore, let K_Σ be the number of distinct locations in $\mathbf{x}_\Sigma = \sum_{m=1}^M \mathbf{x}_m$. If $N \geq 2K_\Sigma$, then $\mathbf{x}_1, \mathbf{x}_2, \dots, \mathbf{x}_M$ can be uniquely recovered from $\mathbf{y}_1, \mathbf{y}_2, \dots, \mathbf{y}_M$.

III. RELATED WORK

Our results from Section II showed that reconstructing multi-channel signals from mismatched samples takes the form

of an unlabeled sensing problem if each signal admits a sparse representation in the continuous domain and the support can be estimated from their addition. This section provides a short overview on related work regarding unlabeled sensing and reconstructing continuous-time sparse signals.

A. Unlabeled Sensing

There has been a considerable amount of research regarding linear regression without correspondences, which can be formulated as a linear system of equations $\mathbf{y} = \mathbf{\Pi}\mathbf{A}\boldsymbol{\beta}$, with the permutation matrix $\mathbf{\Pi}$ and regression coefficients $\boldsymbol{\beta}$ as unknowns (see Corollary 1). In [1], Unnikrishnan *et al.* showed that for a random matrix \mathbf{A} drawn from any continuous probability distribution, $\boldsymbol{\beta}$ can be uniquely recovered w.p. 1 as long as $N \geq 2K$, otherwise the solution is not unique w.p. 1. This result could be generalized to arbitrary invertible and diagonalizable transformation matrices [12] and extended by replacing the permutation with an unknown linear map from a given finite set of linear maps [14]. Further, it was shown that the maximum likelihood estimate (MLE) of $\boldsymbol{\beta}$ for a response vector that is corrupted by additive random noise tends towards the optimal solution for increasing signal to noise ratio (SNR) [1] and the authors in [15] established lower bounds on the SNR below which the estimation error is above a threshold for any estimator. On the other hand, it was shown in [16] that the optimal permutation matrix coincides with high probability with the MLE if the SNR is fixed and exceeds a threshold. However, if the SNR is too low, the MLE differs from the optimal solution with high probability and it could be shown for a fixed SNR that the MLE is asymptotically inconsistent [17]. More recently, it was proven that for a sparsely shuffled response vector the optimal solution coincides with the optimal solution of an ℓ_1 -regression problem [18] which can be solved via convex optimization [18], and by relying on hypothesis testing, expectation maximization (EM) and reweighted least squares [19]. Other EM approaches have been proposed in [20] and were improved upon in [13], where the authors developed an algebraic geometric theory for this problem by expressing it as a polynomial system, which contains the optimal regression coefficients in its root locus. Tsakiris *et al.* also proposed approaches based on branch-and-bound, RANSAC and concave minimization [14], [21]. In [22], the problem was posed as a sparse error correction and solved by means of hard thresholding pursuit. Other approaches for solving unlabeled sensing problems are based on geometric reconstruction [23], observation-specific offsets and ℓ_1 -penalization [24], or graph matching algorithms [25]. More recently, the problem of sample mismatches has been considered for principal component analysis [26], where the authors show that it is well defined and they propose a two-stage solver based on algebraic geometry. In [27], the authors address the problem of learning models that are not necessarily linear by utilizing pairwise comparison data.

B. Continuous-Time Sparse Signal Reconstruction

In [9], Vetterli *et al.* proposed a sampling theorem for a class of sparse signals, e.g., streams of (differentiated) Diracs, piecewise polynomials or nonuniform splines, and they showed

that such signals can be perfectly reconstructed from lowpass filtered samples for some families of sampling kernels, such as ideal lowpass filters and Gaussian kernels. Later, the class of sampling kernels allowing perfect reconstruction was extended to kernels satisfying the so-called Strang-Fix conditions [28] and the theory has been adapted to also include piecewise sinusoidal signals [29] and handle noisy observations [30]. More recently, the conditions for perfect reconstruction for noiseless samples and sampling kernels that satisfy the Strang-Fix conditions was generalized [31] and novel denoising algorithms based on structured low-rank matrix approximation have been developed [31]–[33]. Alternatively, methods based on convex optimization and atomic norm minimization [34], [35] have also been proposed for the estimation of sparse signals in *off-the-grid* settings.

IV. PROPOSED TWO-STEP ESTIMATION APPROACH

In this section, we devise a method for solving the considered problem in the two-channel case. We propose a two-step estimation approach based on the results from Section II. Step 1 is dedicated solely to the estimation of the support of the signals over the continuum from their addition, while Step 2 builds upon this estimate and attempts to solve the resulting unlabeled sensing problem. However, in a practical setting the observations are corrupted with measurement noise. Hence, the signals are modeled as the sum of a deterministic component admitting a sparse representation according to (1) and a random perturbation term that is assumed to be normally distributed, i.e.,

$$\tilde{\mathbf{x}}_m = \mathbf{x}_m + \boldsymbol{\nu}_m, \boldsymbol{\nu}_m \sim \mathcal{N}(0, \sigma_m^2), m = 1, 2. \quad (8)$$

Remark 3. Note that Theorem 1 guarantees a unique recovery of $\tilde{\mathbf{x}}_m$ for all $m = 1, \dots, M$ only if $\sigma_m = 0$. Additionally, the support vectors have to be constructed from the estimated locations of the noisy signals $\{\tilde{\mathbf{x}}_m\}_{m=1}^M$. The estimation errors from Step 1 are reflected in the estimated sensing matrix $\hat{\mathbf{A}}$ as so-called leverage points, while shuffled samples that deviate largely from each other, induce outliers in the residuals with respect to the assumed Gaussian distribution.

Step 1 - Estimating Support: First, the two shuffled measurement vectors $\tilde{\mathbf{y}}_1$ and $\tilde{\mathbf{y}}_2$ with $\tilde{\mathbf{y}} := (\tilde{\mathbf{y}}_1^\top, \tilde{\mathbf{y}}_2^\top)^\top$, $\tilde{\mathbf{x}} := (\tilde{\mathbf{x}}_1^\top, \tilde{\mathbf{x}}_2^\top)^\top$ and $\tilde{\mathbf{y}} := \mathbf{\Pi}_q \tilde{\mathbf{x}}$ as in (3) are added, i.e., $\tilde{\mathbf{y}}_\Sigma = \tilde{\mathbf{x}}_\Sigma = \tilde{\mathbf{x}}_1 + \tilde{\mathbf{x}}_2 = \tilde{\mathbf{y}}_1 + \tilde{\mathbf{y}}_2$, where $\tilde{\mathbf{x}}_1$ and $\tilde{\mathbf{x}}_2$ are the noisy unshuffled measurement vectors as defined in (8). Thus, the sum is given by $\tilde{\mathbf{y}}_\Sigma = \mathbf{y}_\Sigma + \boldsymbol{\nu}_\Sigma$ with $\boldsymbol{\nu}_\Sigma \sim \mathcal{N}(0, \sigma_1^2 + \sigma_2^2)$. To estimate the parameters of the signal mixture one could resort to the methods described in Section III. However, many of these methods rely on the low-rank property of the Toeplitz matrix constructed from the Fourier Series (FS) coefficients of the signal of interest, which is not necessarily present in the case of noisy samples. In our case, we propose to use methods that impose a low-rank constraint on the Toeplitz matrix formed from the sequence of DFT coefficients $[\text{DFT}_N(\tilde{\mathbf{x}}_m)]_\ell$ [36] [32], [31], [33]. These methods can be seen as a denoising step to get a better estimate of the true $X_{\Sigma, \ell}$ prior to the application of a line spectral estimation method (e.g., Prony's method [11]) to

recover the signal parameters. Here, we choose the method in [31] which uses ADMM to solve the denoising problem with low-rank constraints due to its superior performance and faster convergence as compared to [32], [33]. Once we get an estimate of the signal parameters $\hat{\Theta}_\Sigma$ we can form the matrix $\hat{U} = \mathbf{W}\hat{V}_\Sigma$ where \hat{V}_Σ is an estimate of the true V_Σ .

Step 2 - Shuffled Regression: While there are approaches to solve the general unlabeled sensing problem that assume a known sensing matrix [13], [37], [1], [18], [20], [19], [22], to the best of our knowledge, there exists no method that assumes contaminated regressors, while also exploiting the structure of the permutation. Assuming Gaussian noise, for a contamination-free regression matrix (i.e., $\hat{\mathbf{A}} = \mathbf{A}$), the maximum likelihood estimate (MLE) of the structured unlabeled sensing problem is the solution to the problem

$$\begin{aligned} (\hat{\Pi}_{q,\text{ML}}, \hat{\beta}_{\text{ML}}) &= \arg \min_{\Pi_q, \beta} \|\tilde{\mathbf{y}} - \Pi_q \mathbf{A} \beta\|_2^2 \quad (9) \\ \text{s.t. } q_n &\in \{0, 1\}, \beta \in \mathbb{R}^{2K_\Sigma}. \end{aligned}$$

However, we do not have access to \mathbf{A} but rather to an estimate $\hat{\mathbf{A}}$ of it, which violates the assumptions that are required for the MLE to be optimal. Still, if $\hat{\mathbf{A}}$ is sufficiently close to \mathbf{A} , the MLE is a reasonable choice to solve the following problem instead:

$$\begin{aligned} \min_{\Pi_q, \beta} \|\tilde{\mathbf{y}} - \Pi_q \hat{\mathbf{A}} \beta\|_2^2 \quad (10) \\ \text{s.t. } q_n &\in \{0, 1\}, \beta \in \mathbb{R}^{2K_\Sigma}. \end{aligned}$$

The combinatorial nature of problem (10) makes it difficult to solve, and a natural approach is to relax \mathbf{q} to lie in the convex set $[0, 1]^N$. Unfortunately, in any kind of alternate minimization approach, where the regression problem is solved for a previously estimated permutation matrix, the response vector may be contaminated by arbitrary outliers due to the shuffling. It is a well-known fact that these errors lead to a severe drop in performance of the MLE [38], [39], [40], [41]. Robust estimators have been developed as a means to deal with such erroneous data. For the linear regression problem, $\tilde{\mathbf{y}} = \mathbf{H}\beta + \varepsilon$ in particular, the goal is to estimate β even when \mathbf{H} contains outliers and ε is non-Gaussian and possibly heavy-tailed. Given estimates $\hat{\Pi}_q$ and $\hat{\mathbf{A}}$, we can define $\mathbf{H} := \hat{\Pi}_q \hat{\mathbf{A}}$ and solve for β using a robust estimator. In this work, the robust MM-estimator [40] is adopted due to its high breakdown point (maximum proportion of outlier-contamination beyond which its asymptotic bias is infinite) and high asymptotic relative efficiency (ratio of the MM-estimators asymptotic variance compared to that of the Gaussian MLE for normally distributed noise) for normally distributed residuals [41]. To achieve a high breakdown point and maintain high efficiency, MM-estimators [40] are calculated in two steps. First, a high breakdown point estimate is computed, e.g., an S-estimate [42], which is given by

$$\hat{\beta}_S = \underset{\beta}{\operatorname{argmin}} \hat{\sigma}(\mathbf{r}),$$

Algorithm 1 Proposed Method

Input: $\tilde{\mathbf{y}}_1, \tilde{\mathbf{y}}_2 \in \mathbb{R}^N$, $K_\Sigma > 2$, $\text{maxiter} > 0$

- 1: Initialize: $\hat{\mathbf{q}} = (1, \dots, 1)^\top$, $\hat{\Pi}_q$ according to (3), $\tilde{\mathbf{y}} = (\tilde{\mathbf{y}}_1^\top, \tilde{\mathbf{y}}_2^\top)^\top$, $\hat{\mathbf{x}} = \hat{\Pi}_q^\top \tilde{\mathbf{y}}$
- 2: $\hat{X}_{\Sigma, \ell} \leftarrow$ DFT and denoise $(\tilde{\mathbf{y}}_1 + \tilde{\mathbf{y}}_2)$ [31]
- 3: $\{\hat{t}_k\}_{k=0}^{K_\Sigma-1} \leftarrow$ Line spectral estimation of $\hat{X}_{\Sigma, \ell}$ [11]
- 4: $\hat{\mathbf{A}} \leftarrow \operatorname{diag}(\hat{U})$, \hat{U} from $\{\hat{t}_k\}_{k=0}^{K_\Sigma-1}$ according to $\hat{U} = \mathbf{W}\hat{V}_\Sigma$
- 5: **while** $\text{iter} \leq \text{maxiter}$ **do**:
- 6: $\hat{\beta}_{\text{MM}} \leftarrow$ Robust MM-estimate of linear regression $\hat{\mathbf{x}} = \hat{\mathbf{A}}\beta + \varepsilon$ [40]
- 7: $\hat{\mathbf{q}} \leftarrow \operatorname{proj}_{\{0,1\}} \left(\underset{\mathbf{q}, q_n \in [0,1]}{\operatorname{argmin}} \|\hat{\Pi}_q^\top \tilde{\mathbf{y}} - \hat{\mathbf{A}}\hat{\beta}_{\text{MM}}\|_2^2 \right)$
- 8: $\hat{\mathbf{x}} \leftarrow \hat{\Pi}_q^\top \tilde{\mathbf{y}}$
- 9: $\text{iter} \leftarrow \text{iter} + 1$
- 10: Select $\hat{\beta}$, $\hat{\mathbf{q}}$ with smallest MSE = $\|\hat{\Pi}_q^\top \tilde{\mathbf{y}} - \hat{\mathbf{A}}\hat{\beta}_{\text{MM}}\|_2^2$

Output: $\hat{\mathbf{A}}$, $\hat{\beta}$, $\hat{\mathbf{q}}$

where $\mathbf{r} = (r_1, \dots, r_N)^\top$ with $r_i = \tilde{y}_i - \hat{\mathbf{a}}_{[i]}^\top \beta$ ($\hat{\mathbf{a}}_{[i]}^\top$ is the i th row vector of $\hat{\mathbf{A}}$) and $\hat{\sigma}(\tilde{y}_i - \hat{\mathbf{a}}_{[i]}^\top \beta)$ is the M-scale estimate defined as the solution to

$$\frac{1}{N} \sum_{i=1}^N \rho_1 \left(\frac{r_i}{\hat{\sigma}} \right) = \delta,$$

for a robust loss function ρ_1 satisfying the assumptions A1 in [40], a given β and $0 < \delta < \rho_1(\infty)$, where, for consistency at the Gaussian distribution, δ is the expected value of $\rho_1(u)$ with u being a standard Gaussian random variable [38]. If the loss function ρ_1 is taken to be Tukey's biweight loss function (see Fig. 3)

$$\rho_{\text{Tuk}}(x) = \begin{cases} \frac{c^2}{6} \left(1 - \left(1 - \frac{x^2}{c^2} \right)^3 \right) & |x| \leq c \\ \frac{c^2}{6} & |x| > c, \end{cases}$$

the S-estimator can attain a breakdown point of 0.5, if c is chosen as 1.548 [43]. However, for this choice of c , it achieves an asymptotic relative efficiency of only 0.29 for normally distributed errors. Thus, the estimate $\hat{\beta}_S$ and the corresponding residual scale $\hat{\sigma}_S$ are used as initializers for a redescending M-estimator of regression with robust loss

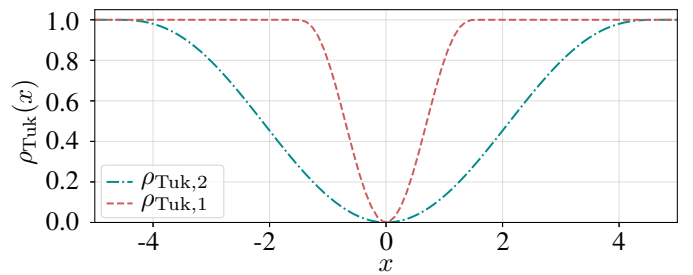


Fig. 3. Exemplary plots of Tukey's biweight loss functions $\rho_{\text{Tuk},1}$ and $\rho_{\text{Tuk},2}$ with respective tuning parameters $c_1 = 1.548$ and $c_2 = 4.685$. The functions are normalized such that $\sup(\rho_{\text{Tuk},1}) = \sup(\rho_{\text{Tuk},2}) = 1$.

function ρ_2 that has been tuned for high efficiency. In more concrete terms, the MM-estimator achieves an asymptotic relative efficiency of 0.95, if $\rho_2 = \rho_{\text{Tuk}}$ with $c = 4.685$ [40]. It is then given by

$$\hat{\beta}_{\text{MM}} = \underset{\beta}{\operatorname{argmin}} \sum_{i=1}^N \rho_2 \left(\frac{y_i - \mathbf{a}_{[i]}^\top \beta}{\hat{\sigma}_S} \right),$$

which can be computed by means of the iteratively reweighted least-squares (IRWLS) algorithm and where it is necessary that $\rho_2(r) \leq \rho_1(r)$ [40]. After initializing $\hat{\mathbf{q}} = (1, \dots, 1)$ and $\hat{\mathbf{x}} = \hat{\Pi}_q^\top \hat{\mathbf{y}}$, where $\hat{\Pi}_q$ is constructed from $\hat{\mathbf{q}}$ following the definition in (3), the MM-estimate $\hat{\beta}_{\text{MM}}$ is computed w.r.t. $\hat{\mathbf{x}}$. Then, the convex program

$$\begin{aligned} \hat{\mathbf{q}}_{[0,1]} &= \underset{\mathbf{q}}{\operatorname{argmin}} \|\hat{\mathbf{y}} - \Pi_q \hat{\mathbf{A}} \hat{\beta}_{\text{MM}}\|_2^2, \\ \text{s.t. } q_n &\in [0, 1], \end{aligned} \quad (11)$$

is evaluated and the estimate $\hat{\mathbf{q}}_{[0,1]}$ is projected onto the binary set $\{0, 1\}^N$, i.e., $\hat{\mathbf{q}} = \operatorname{proj}_{\{0,1\}}(\hat{\mathbf{q}}_{[0,1]})$, which serves as a proxy for the true assignment vector \mathbf{q} . Again, from $\hat{\mathbf{q}}$ the matrix $\hat{\Pi}_q$ is constructed and the measurements are permuted according to $\hat{\mathbf{x}} = \hat{\Pi}_q^\top \mathbf{y}$. Unfortunately, iterating this approach does not guarantee convergence, due to the nonconvexity of the MM-estimator as well as the binary projection. However, since the MM-estimator has a high breakdown point, making a few mistakes in the sample assignment has a small impact on the estimated model. Therefore, the process is repeated until some predefined number of maximum iterations is reached. Then from all iterations, the assignment vector $\hat{\mathbf{q}}$ and the regression coefficients $\hat{\beta}_{\text{MM}}$ with smallest MSE = $\|\hat{\Pi}_q^\top \mathbf{y} - \hat{\mathbf{A}} \hat{\beta}_{\text{MM}}\|_2^2$ are selected. Note that in (11), the residual sum of squares is minimized instead of a robust loss, since $\hat{\mathbf{x}} = \hat{\mathbf{A}} \hat{\beta}_{\text{MM}}$ is already a robust estimate of the true signals and for the optimal permutation, the residuals are assumed to be normally distributed, i.e., free of outliers.

V. EXPERIMENTAL EVALUATION

A. Application in Computational Neuroscience

We evaluate the proposed approach for an application in computational neuroscience related to whole brain calcium imaging. Calcium imaging refers to a technique that allows to measure the firing activity of large populations of neurons by means of fluorescent calcium indicators [44]. When a neuron produces an action potential there is an exchange of calcium ions across the cell membrane resulting in an increase of calcium concentration $[\text{Ca}^{+2}]$ in the cell body. These fluorescent markers bind to calcium ions and therefore allow us to measure a surrogate of a neuron's firing activity. The observed fluorescent traces can be well-approximated as a stream of decaying exponentials [44], [45]. We rely on this model and assume that the continuous-time fluorescent trace of a neuron $z(t)$ can be modelled as the convolution of a periodic stream of K Dirac delta functions with a normalized period of one $s(t)$ and a causal decaying exponential shaping kernel $g(t)$ as:

$$z(t) = s(t) * g(t) = \sum_{i \in \mathbb{Z}} \sum_{k=0}^{K-1} a_k \delta(t - t_k - i) * e^{-\alpha t} u(t), \quad (12)$$

where $a_k \in \mathbb{R}_+$ and $t_k \in [0, 1)$ correspond to the amplitudes and firing instants of the neuron, $\delta(t)$ ¹ is the Dirac delta function, $u(t)$ is the unit-step function, and $\alpha > 0$ is the decay factor of the exponential. Note that the FS coefficients of $z(t)$ are given by $Z_\ell = S_\ell / (\alpha + j2\pi\ell)$ for $\ell \in \mathbb{Z}$ where $S_\ell = \sum_k a_k e^{-j2\pi\ell t_k}$ correspond to the FS coefficients of the stream of Diracs which follows the model in (1). Using the sampling setup in Fig. 2 and assuming that the sampling kernel $\varphi(t)$ is an ideal low-pass filter it can be shown [46] that the sequence of samples $x_n = z(t) * \varphi(-t)|_{t=n}$, $n = 0, \dots, N-1$ has a DFT that coincides with the FS coefficients of $z(t)$, that is $[\text{DFT}_N(\mathbf{x})]_\ell = \sum_n z_n e^{-j2\pi n \ell / N} = Z_\ell$. Since the exponential shaping filter does not have any zeros in the frequency domain the proposed approach can still be applied. The only modification in Algorithm 1 is that we need to compensate for the attenuation of the FS coefficients introduced by the shaping kernel $g(t)$. More precisely, given shuffled multi-channel observations the estimate of the FS coefficients of the sparse signal (prior to denoising) is computed as:

$$\begin{aligned} \hat{S}_{\Sigma, \ell} &= (\alpha + j2\pi\ell) [\text{DFT}_N(\hat{\mathbf{y}}_\Sigma)]_\ell \\ &= (\alpha + j2\pi\ell) \hat{X}_{\Sigma, \ell}, \quad \ell = 0, \dots, N-1. \end{aligned} \quad (13)$$

After denoising $\hat{S}_{\Sigma, \ell}$, a line spectral estimation method can be applied to estimate the locations $t_{\Sigma, k}$ (and hence the sensing matrix) as discussed in Section IV. Note that in this case, the matrix $\hat{\mathbf{U}}$ is given as $\hat{\mathbf{U}} = \mathbf{W} \Psi \hat{\mathbf{V}}_\Sigma$, where Ψ is a diagonal matrix of appropriate dimensions with elements $1/(\alpha + j2\pi\ell)$.

B. Performance Metrics

For evaluating the performance of the proposed method we consider two different aspects: the signal reconstruction error, and the sample assignment. For the signal reconstruction, the normalized mean squared error (nMSE) is adopted in order to compare signals with different strength/norm. To assess the performance of the sample assignment, we use the binary accuracy weighted by the the absolute deviations of the two unshuffled and noiseless signals $\mathbf{x}_1, \mathbf{x}_2$. For real traces, the deviations are computed with respect to the unshuffled but noisy signals. Let \mathcal{A} denote the set of indices of correctly assigned samples; the weighted accuracy (WA) and the nMSE are then given by

$$\text{WA} = \frac{\sum_{n' \in \mathcal{A}} |x_{1, n'} - x_{2, n'}|}{\sum_{n=1}^N |x_{1, n} - x_{2, n}|}, \quad \text{nMSE} = \frac{\|\mathbf{x} - \hat{\mathbf{A}} \hat{\beta}\|_2^2}{\|\mathbf{x}\|_2^2}.$$

An important notion regarding both metrics is that the ordering of channels in the estimated signals is ambiguous. This means that we have to compute the metrics with respect to both orderings and then select the better result. More concretely, the nMSE has to be computed with respect to the vectors $(\mathbf{x}_1^\top, \mathbf{x}_2^\top)^\top$ and $(\mathbf{x}_2^\top, \mathbf{x}_1^\top)^\top$, respectively, while the correct assignments in the WA have to be determined with respect to \mathbf{q} and $(\mathbf{1} - \mathbf{q})$, where $\mathbf{1} = (1, 1, \dots, 1)^\top$. Then, the smaller nMSE and the larger WA are selected.

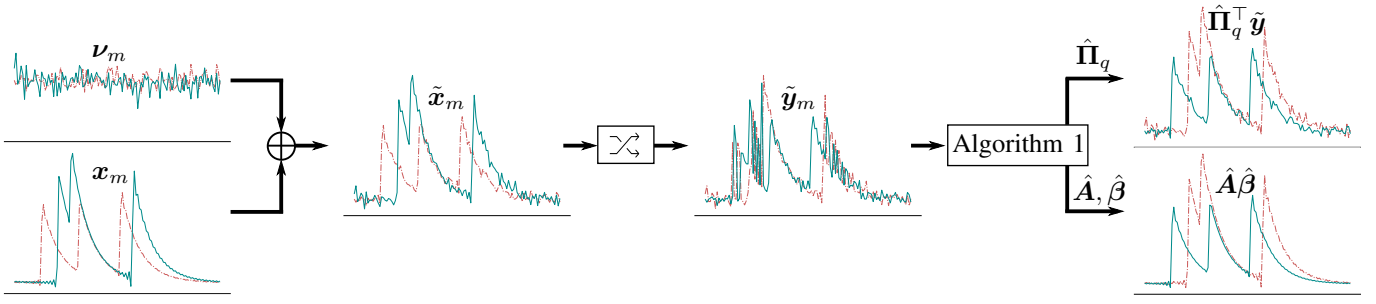


Fig. 4. **Illustration of the experiment pipeline:** The ground truth signals x_m are generated according to some specified locations, amplitudes and decay parameter. After adding zero-mean white Gaussian noise v_m the signals are shuffled, resulting in the measurement vectors \tilde{y}_m . Then, the proposed method is applied in order to reconstruct the signals $(\hat{A}\hat{\beta})$ and assign the samples to their respective channels $(\hat{\Pi}_q^T \tilde{y})$.

C. Numerical Experiments

Experiment Pipeline: The experiment pipeline, including signal generation and estimation, is illustrated in Fig. 4. The signal generation, generally speaking, follows the same basic procedure. For some initialized numbers of Diracs K_1 and K_2 , associated locations t_k and amplitudes a_k as well as a fixed decay parameter α (presumed to be known), the two sample sequences $x_{1,n}$ and $x_{2,n}$ of the one-periodic streams of decaying exponentials are given by the DFT of their respective sequence of FS coefficients defined in (1). The locations t_k are sampled without replacement from a discrete uniform distribution on the grid between 0 and 1 with a spacing of $\Delta t = 0.02$ to ensure that, for estimated parameters $\hat{\Theta}$, the regression matrix does not become too ill-conditioned since, in theory, two Diracs can be placed arbitrarily close together.

Remark 4. Note that although the locations t_k are generated on a grid for simplicity, this information is not exploited in the estimation of the support and the proposed method can be applied in the same manner to signals, where the locations lie off the grid, e.g., the signals generated in Section V-D.

Remark 5. Further, note that the locations are sampled for both signals individually. Thus, two Diracs may occur at the same time, which means that the signals may very well have overlapping support. However, this does not pose a problem, since in this case the sensing matrix U still has full column rank.

The corresponding amplitudes a_k are sampled from a continuous uniform distribution on the closed interval $[0.5, 1]$. Determining an appropriate number of Diracs and decay factor α is highly dependent on the method and the true sampling rate of the acquisition process. Here, the signal generation is adapted to the use-case of signals that can be observed in the fluorescent traces that result from calcium imaging experiments of spiking neurons. These signals have been successfully described as FRI signals with a decaying exponential kernel [46], [47] and give a reasonable range for the parameters. A common sampling rate in calcium imaging is $f_s = 30$ Hz, which we will assume in our experiments. A thorough analysis of the intensity half-life $\tau_{1/2}$ for different fluorescent proteins has been conducted, e.g., in [44] and

shows that the half-life ranges between 0.2 s and 1 s depending on the neuron's firing rate and the used fluorescent protein. Since our signal model assumes a canonical period of $T = 1$ and, thus, the sampling rate of the model corresponds to the sample size N , α is computed from f_s , N and $\tau_{1/2}$ as

$$\alpha = \ln(2) \frac{N}{\tau_{1/2} f_s}. \quad (14)$$

After the noiseless and unshuffled signals have been generated, they are corrupted by additive white Gaussian noise with a target SNR in dB resulting in the unshuffled sample vectors $\tilde{x}_m, m = 1, 2$. The noise variances σ_m^2 are calculated as

$$\sigma_m^2 = 10^{\frac{\text{SNR} - P_m}{10}}, P_m = 10 \log_{10} \left(\frac{1}{N} \sum_{n=0}^{N-1} x_{m,n}^2 \right), \quad (15)$$

where P_m is the average signal power. Finally, the assignment vector q of the noisy signals can be generated randomly or as a structured vector, where the percentage of shuffled samples is determined by the ratio of zero and nonzero elements in q . Then, the shuffled sample vectors are computed as $(\tilde{y}_1^T, \tilde{y}_2^T)^T = \Pi_q (\tilde{x}_1^T, \tilde{x}_2^T)^T$.

Known versus Estimated Support: In the first set of experiments, we analyze the effect of error propagation in the two-step approach. The signals are generated according to the model in (12) but scaled in time to span 3s per period. Each signal is composed of 3 exponentials with a decay parameter $\alpha = 11.18$ (corresponding half-life $\tau_{1/2} = 0.25$ s); the number of samples is $N = 121$ out of which between 2 and 58 (i.e., up to 50 %) are randomly shuffled; the Signal to Noise Ratio (SNR) ranges from 20 dB to 50 dB in 10 dB steps. The results are averaged over 1000 random realizations for each number of shuffled samples. Fig. 5 (a) shows the performance of the method when the support is known, whereas the Fig. 5 (b) displays the performance for an estimated support but otherwise equivalent setting. In both figures, a phase transition of the median and the percentiles of the nMSE can be observed. As the SNR increases, this phase transition occurs for increasing proportions of shuffled samples and in the case of known support and at very high SNR it does not occur at all. Although it is expected that this phase transition will occur earlier when the support is estimated than when it is known, comparing Fig. 5 (a) and (b) shows that this effect is in fact very small since the MM-estimator is robust to errors in the regressors. On average,

$$^1 \int_{-\infty}^{\infty} f(t) \delta(t - t_0) dt = f(t_0), \quad \int_{-\infty}^{\infty} \delta(t) dt = 1$$

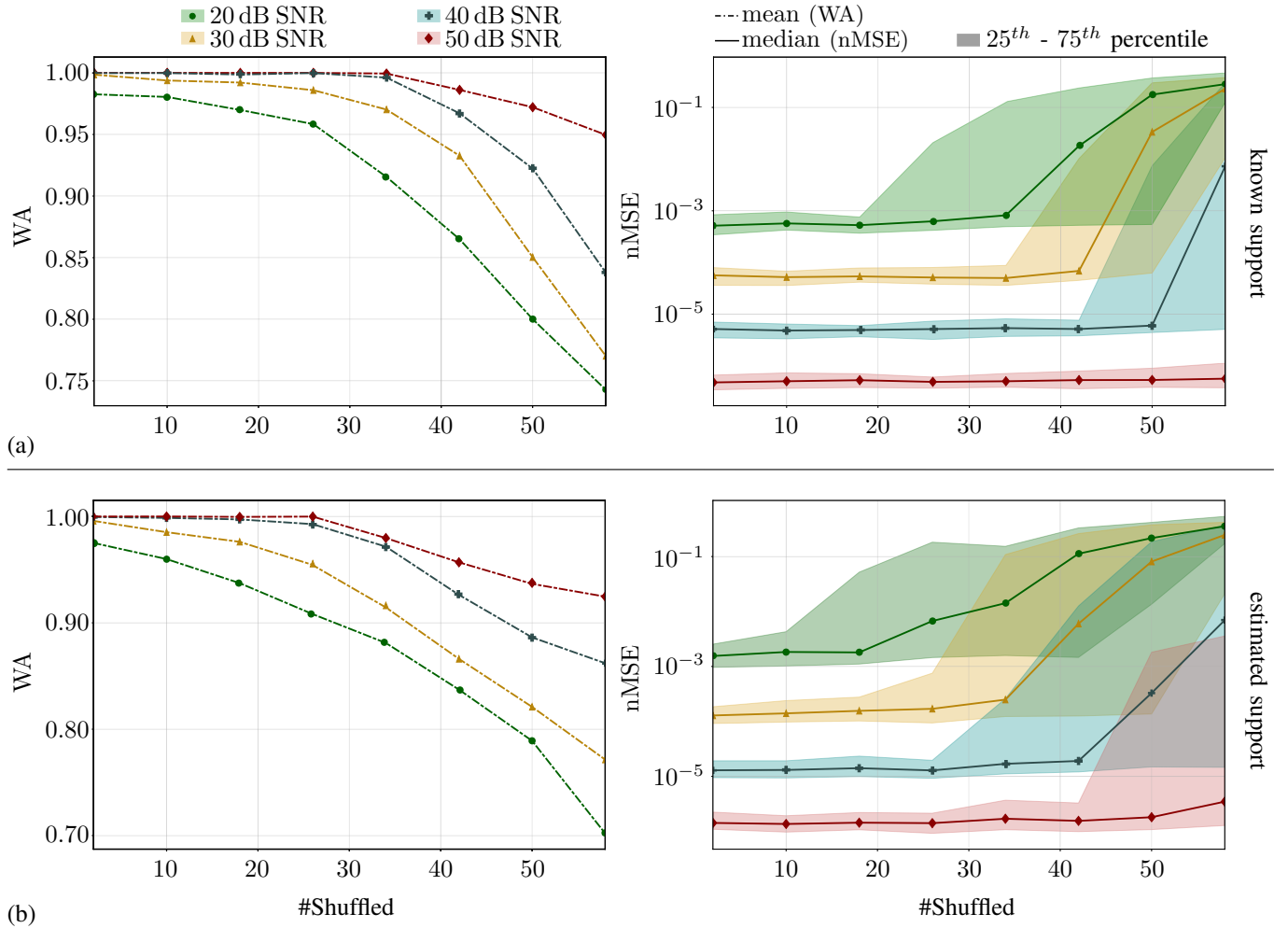


Fig. 5. **Random shuffle for known (a) and estimated locations (b):** Performance for different levels of SNR and varying numbers of shuffled samples. The left plots show the mean weighted accuracy (WA), while the right plot shows the median nMSE as well as 25th and 75th percentile for the following parameters: $K_1 = 3$, $K_2 = 3$, $\tau_{1/2} = 0.25$ s ($\alpha = 11.18$), $N = 121$.

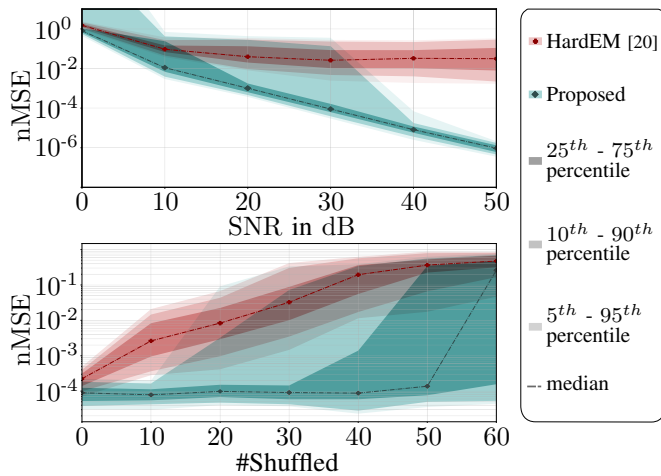


Fig. 6. **Benchmark:** Comparison of proposed method and HardEM [20] (red) for estimated locations in terms of nMSE. In the top plot, $\approx 25\%$ of the samples have been shuffled for varying SNR. In the bottom plot, the SNR is fixed to 30 dB, while the number of shuffled samples varies. The signals are generated according to the following parameters: $K_1 = 2$, $K_2 = 2$, $\tau_{1/2} = 0.25$ s ($\alpha = 11.18$), $N = 121$.

the proposed method is able to produce satisfactory results in terms of signal reconstruction and sample assignments up to $\approx 25\%$ shuffled samples for $\text{SNR} \geq 20$ dB and up to $\approx 33.3\%$ shuffled samples for $\text{SNR} \geq 30$ dB for both, known and estimated support.

Benchmark: Two experiments comparing the proposed robust estimation method against the HardEM algorithm [20] for shuffled linear regression have been conducted, by replacing the shuffled regression step of the proposed algorithm (treating $\hat{\mathbf{A}}$ as \mathbf{A}) with the HardEM algorithm. The HardEM algorithm has been proposed as an approach to solve a shuffled regression problem for general permutation matrices, hence it does not take advantage of the known structure on the permutation matrices that is given in our setup. Thus, only the nMSE is considered as evaluation metric since the WA has not been defined for general permutations. The signal generation follows the same input parameters as before, except that $K_1 = K_2 = 2$, aiming to keep the comparison between the two methods fair since the HardEM algorithm (as well as other methods) do not perform well, if the dimensionality of the problem increases [13], [20], [22]. In the first experiment, 30 samples ($\approx 25\%$) are randomly shuffled with the SNR

ranging from 0 dB to 50 dB. In the second experiment, the number of randomly shuffled samples increases for a fixed SNR = 30 dB. The performance of both methods is displayed in Fig. 6, where the left plot shows the nMSE for a fixed number of 30 shuffled samples and varying SNR and the right plot displays the nMSE for a fixed SNR and varying numbers of shuffled samples. While the average performance of the HardEM method already begins to deteriorate for 10 shuffled samples, the average nMSE of the proposed Method does not increase significantly until more than 30 samples are shuffled. On a similar note, for increasing SNR the average nMSE of the HardEM method saturates around 10^{-2} , while for the proposed method it decreases by a constant factor of approximately 10^{-1} per 10 dB increase in SNR.

D. Refinement and Lower Bounds

A natural approach to possibly increase the performance of the proposed method is to introduce an additional refinement step in which the support is estimated from individual channels with reassigned samples according to the estimate $\hat{\mathbf{\Pi}}_q$ resulting from Algorithm 1. This new estimate of the matrix \mathbf{A} and the reassigned samples provide then the input to Step 2 of the proposed method, i.e., the robust iterative approach to solving the unlabeled sensing problem. This section addresses this by comparing such a refinement with the estimate from Algorithm 1 and with the estimate using spectral line estimation on $\tilde{\mathbf{x}}_1$, $\tilde{\mathbf{x}}_2$, which provides a lower bound on the performance of the proposed methods. The evaluation takes into account the performance on estimating the support of the signals as well as the signal reconstruction.

In the conducted experiments, each signal consists of two Diracs with locations that are sampled uniformly on the interval $[0, 1)$ with the constraint that all K_Σ locations are separated at least by a minimum separation Δt in order to avoid arbitrarily ill-conditioned problems. In our experimental setting, a value of $\Delta t = 0.02$ could be observed to be sufficient for stable recovery of the support and is hence chosen for further analysis. Tighter bounds on Δt that still guarantee stable recovery are established in [34], but are not further considered in this work. The amplitudes are sampled uniformly on the interval $[0.5, 1]$. The sample size and the decay parameter are set to $N = 121$ and $\alpha = 11.18$ ($\tau_{1/2} = 0.25$ s), while 30 ($\approx 25\%$) and 40 ($\approx 33\%$) samples are shuffled, respectively. The samples are shuffled at random and the SNR ranges from 0 dB to 50 dB with 1000 realizations per trial. The results are shown in Fig. 7, where the left plots correspond to $\approx 25\%$ samples being shuffled and the right plots correspond to $\approx 33\%$.

In Fig. 7 (a), the weighted accuracy of the estimated assignment resulting from applying Algorithm 1 to $\tilde{\mathbf{y}}$ is shown. These results confirm the observations made in previous experiments, i.e., the accuracy of the assignment increases significantly as the SNR increases. It approaches a perfect assignment for very high SNR, but saturates later when more samples are shuffled.

Fig. 7 (b) shows the nMSE of the estimated locations resulting from applying the ADMM denoising and Prony's

method to individual unshuffled samples $\tilde{\mathbf{x}}_1$, $\tilde{\mathbf{x}}_2$ (brown triangles), added samples $\tilde{\mathbf{y}}_\Sigma$ (red circles) and reassigned individual samples $\hat{\mathbf{x}}_1 = \hat{\mathbf{Q}}\tilde{\mathbf{y}}_1 + (\mathbf{I} - \hat{\mathbf{Q}})\tilde{\mathbf{y}}_2$, $\hat{\mathbf{x}}_2 = \hat{\mathbf{Q}}\tilde{\mathbf{y}}_2 + (\mathbf{I} - \hat{\mathbf{Q}})\tilde{\mathbf{y}}_1$ (blue crosses). For any SNR ≥ 10 dB, the estimation error for individual channels is approximately half of the nMSE for estimates using $\tilde{\mathbf{x}}_\Sigma$, i.e., the refinement leads at best to a 3 dB gain. Indeed, we observe that the median nMSE of the estimated locations from reassigned samples approaches the lower bound as the SNR increases and reaches it earlier for less shuffled samples. For 33% shuffled samples, there is more variation for moderate to low levels of noise, which appears to correlate with the variation in the performance of the reassignment.

Fig. 7 (c) shows the performance of the entire signal reconstruction, when samples are correctly assigned and the support is estimated from $\tilde{\mathbf{x}}_1$, $\tilde{\mathbf{x}}_2$ (brown triangles), Algorithm 1 is applied to shuffled samples $\tilde{\mathbf{y}}$ (red circles) and when these results have been refined by estimating the support from reassigned samples $\hat{\mathbf{x}}_1$, $\hat{\mathbf{x}}_2$, which serve together with the estimated support as input to Step 2 (unlabeled sensing) of Algorithm 1 (blue crosses). Similar to the support estimation, the refinement leads at most to a 3 dB gain. However, due to the propagation of errors between Step 1 and Step 2 of the proposed method, we observe larger variation in the performance of Algorithm 1 and its refinement. In particular, for 33% shuffled samples a phase transition in the median nMSE occurs between 20 dB and 30 dB. Further, the nMSE shows high variation even at 30 dB and the lower bound is approached by the assignment for ≥ 40 dB. In contrast, the median nMSE of the refinement for 25% shuffled samples tends towards the lower bound for ≥ 10 dB with a significant drop in the variation of the nMSE for ≥ 30 dB.

Although these experiments show that for moderate amounts of shuffled samples and noise as well as larger amounts of shuffled samples and high SNR, a refinement does lead to an increase in performance of signal reconstruction, the gain to be made is at most 3 dB. Compared to the increase in computational cost, this increase in performance is incremental at best and the refinement may even lead to a decrease in performance. It can be argued that, at least in the two-channel case, there is only a 3 dB loss in performance compared to the case of samples not being shuffled. Note that for $M > 2$ signals the loss in performance may be larger due to the oversampling factor (in the unshuffled case) increasing as a multiple of M and for equal noise variances $\sigma_\Sigma^2 = \sum_m \sigma_m^2 = M\sigma_1^2$. However, such an analysis is beyond the scope of this work.

E. Artificially Shuffled Real Data

In this section, we apply the proposed method on artificially shuffled calcium imaging traces from mice taken from the cai-1 dataset [48]. Before beginning the estimation, we initially subtract the baselines of the individual signals. The dataset includes simultaneous electrophysiological recordings, from which the spike counts are extracted. Then, α is estimated from the sum of the signals by means of the golden section search algorithm as described in [46]. With this estimate for

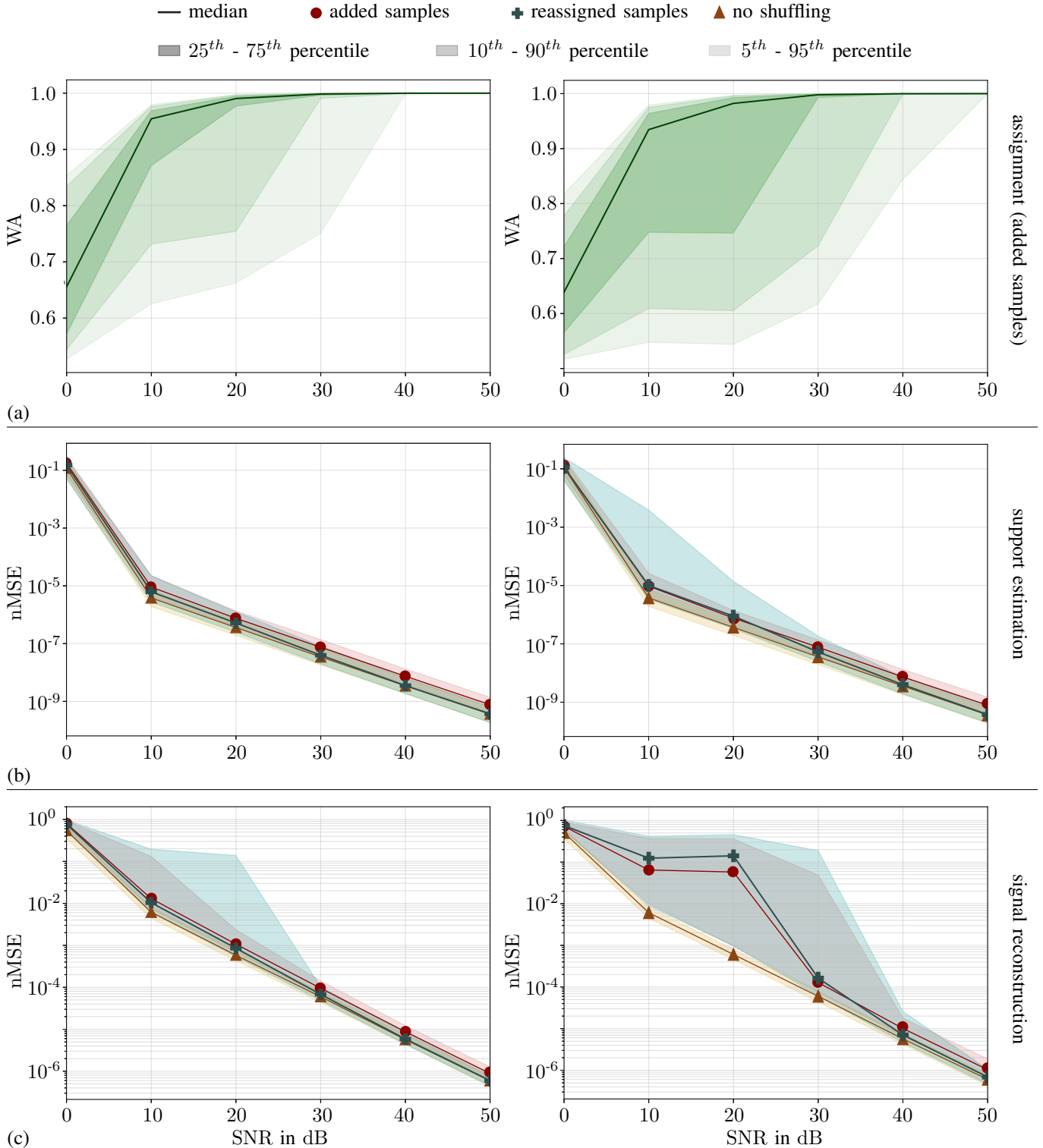


Fig. 7. **Refinement and lower bounds:** Left and right plots correspond to approximately 25% and 33% shuffled samples, respectively. (a) Resulting weighted accuracy by applying Algorithm 1, i.e., acquired sample vectors are added. (b) Normalized MSE of the estimated support using unshuffled individual sample vectors (brown triangles), added sample vectors (red circles) and reassigned individual sample vectors according to the estimated assignment (blue crosses). (c) Signal reconstruction errors when: sample vectors are not shuffled (brown triangles); Algorithm 1 is applied to shuffled sample vectors, i.e., the support is estimated from added samples (red circles); Step 2 (unlabeled sensing) of Algorithm 1 is applied to reassigned samples and the support is estimated from individual channels after the reassignment. The signals were generated according to the following parameters: $K_1 = 2$, $K_2 = 2$, $\tau_{1/2} = 0.25$ s ($\alpha = 11.18$), $N = 121$. Here, the locations $t_k \in [0, 1)$ are continuous uniformly distributed random variables with the constraint of being separated by at least $\Delta t = 0.02$.

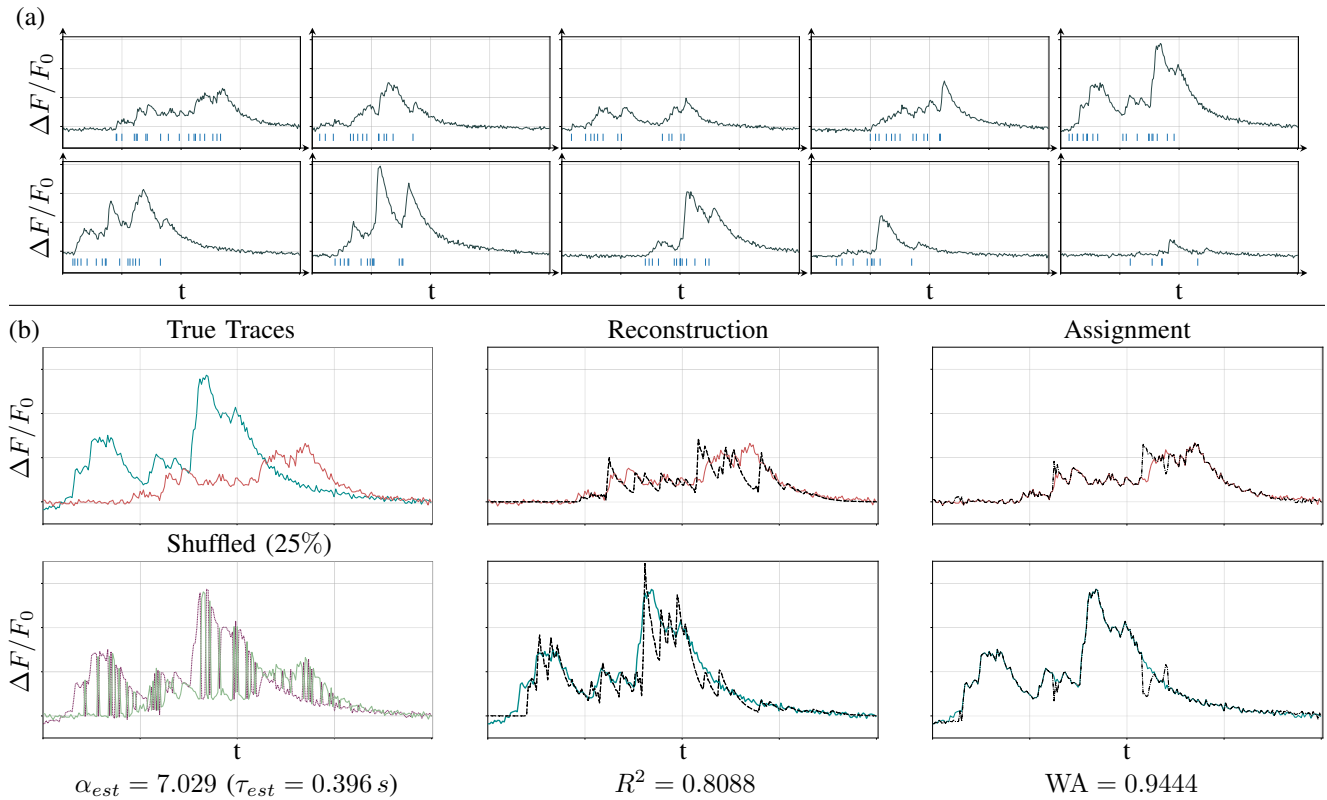


Fig. 8. **Artificially shuffled real data:** (a) Collection of approx. 4 s long windows of true traces (relative intensity of the fluorescent traces $\Delta F/F_0$). Blue vertical bars show the locations of action potentials extracted from electrophysiological recordings; (b) Example of two randomly selected unshuffled traces given by green and red solid lines (top left). Specified amount of samples are shuffled at random (bottom left); Example of reconstructed signals with associated R^2 given by dashed lines (middle); Example of estimated sample assignment with associated WA given by dashed-dotted lines (right).

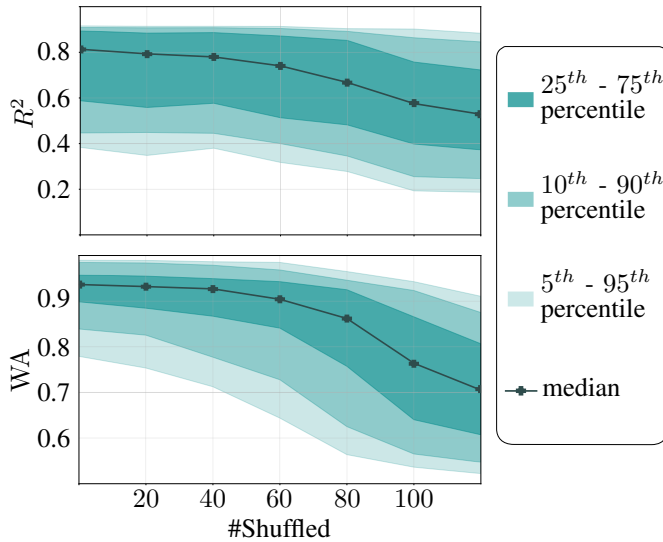


Fig. 9. **Artificially shuffled real data - results:** Average results for 1000 Monte Carlo runs for different amounts of shuffled samples. Top plot shows the median and percentiles of the R^2 , while the bottom plot shows the WA.

the decay and the extracted spike counts K_Σ , the proposed two-step estimation method can be used to estimate the signals and unshuffle the samples. It is important to mention that for this application the amplitudes of the spikes can only take nonnegative values. However, the MM-estimator as an

unconstrained estimator may yield some negative coefficients due to the presence of noise. Simply forcing these coefficients to zero results, however, in a bad fit of the estimated signals ($R^2 \approx 0.2$). Instead, we enforce nonnegativity by replacing the least squares solution in each iteration of the IRWLS algorithm with a nonnegative LS solution. Fig. 8 (a) shows the traces that are used in the experiment. Each trace consists of 241 samples; at a sampling frequency of 60 Hz this yields a length of approximately 4 s. In each trial, two traces are selected randomly from this set and shuffled at random according to the specified number of shuffled samples which is illustrated in the left plots of Fig. 8 (b). Then, the proposed method is applied on the resulting shuffled traces, to return an assignment of the samples and an estimate of the true signals, as shown in the middle and right plots of Fig. 8 (b). Since the true signals are unknown, we report the R^2 as a measure of the signal fit and the weights of the WA are computed w.r.t. the traces. The average results for 1000 trials are shown in Fig. 9, where the amount of shuffled samples is varied. It can be observed that, on average, the method shows satisfactory performance up to 80 shuffled samples ($\approx 33\%$), which matches the observations made in the numerical simulations for moderate levels of noise. Interestingly, the method performs quite well in terms of sample assignment even when disagreements between the estimated model and the true signals can be observed. This implies that the assignment in the two-channel case can tolerate even somewhat larger deviations in the estimated

model as long as sufficient discrimination between the two signals is provided.

VI. CONCLUSION

We introduced a novel framework for the estimation of shuffled multi-channel signals and showed that the problem admits a unique solution. Furthermore, we proposed a two-step estimation procedure that combines sparse signal estimation and robust regression and illustrated its effectiveness in an application related to calcium imaging. Our methodology could be generalized to sparse signal representations other than the ones considered in this work and find application in a variety of real-world problems, such as multiple target tracking or contactless vital signs monitoring of multiple people, where imprecise measurement and channel assignments are present. However, further work needs to be done in order to establish performance guarantees and to consider more challenging scenarios involving a larger number of signals.

REFERENCES

- [1] J. Unnikrishnan, S. Haghghatshoar, and M. Vetterli, "Unlabeled Sensing With Random Linear Measurements," *IEEE Transactions on Information Theory*, vol. 64, pp. 3237–3253, May 2018.
- [2] T. Long, C. Hu, R. Wang, T. Zhang, S. Kong, W. Li, J. Cai, W. Tian, and T. Zeng, "Entomological Radar Overview: System and Signal Processing," *IEEE Aerospace and Electronic Systems Magazine*, vol. 35, pp. 20–32, Jan. 2020.
- [3] F. W. Schenk, N. Brill, U. Marx, D. Hardt, N. König, and R. Schmitt, "High-speed microscopy of continuously moving cell culture vessels," *Scientific Reports*, vol. 6, p. 34038, Sept. 2016.
- [4] J. Brijs, E. Sandblom, M. Axelsson, K. Sundell, H. Sundh, A. Kiessling, C. Berg, and A. Gräns, "Remote physiological monitoring provides unique insights on the cardiovascular performance and stress responses of freely swimming rainbow trout in aquaculture," *Scientific Reports*, vol. 9, p. 9090, June 2019.
- [5] X. Liu, J. Fromm, S. Patel, and D. McDuff, "Multi-task temporal shift attention networks for on-device contactless vitals measurement," in *Advances in Neural Information Processing Systems*, vol. 33, pp. 19400–19411, Curran Associates, Inc., 2020.
- [6] J. Yan, J. Dai, W. Pu, H. Liu, and M. Grec, "Target capacity based resource optimization for multiple target tracking in radar network," *IEEE Transactions on Signal Processing*, vol. 69, pp. 2410–2421, Jan. 2021.
- [7] T. Freweyni K., M. Muma, and A. M. Zoubir, "Adaptive diffusion-based track assisted multi-object labeling in distributed camera networks," in *25th European Signal Processing Conference (EUSIPCO)*, pp. 2299–2303, 2017.
- [8] L. Cong, Z. Wang, Y. Chai, W. Hang, C. Shang, W. Yang, L. Bai, J. Du, K. Wang, and Q. Wen, "Rapid whole brain imaging of neural activity in freely behaving larval zebrafish (*Danio rerio*)," *eLife*, vol. 6, p. e28158, Sept. 2017.
- [9] M. Vetterli, P. Marziliano, and T. Blu, "Sampling signals with finite rate of innovation," *IEEE Transactions on Signal Processing*, vol. 50, pp. 1417–1428, June 2002.
- [10] P. Stoica and R. L. Moses, *Spectral analysis of signals*. Prentice Hall, Upper Saddle River, New Jersey, 1 edition, 2004.
- [11] R. Prony, "Essai expérimental et analytique: sur les lois de la dilatabilité de fluides élastique et sur celles de la force expansive de la vapeur de l'alkool, à différentes températures," *Journal de l'École Polytechnique Floréal et Plairial*, vol. 1, no. 22, pp. 24–76, 1795.
- [12] I. Dokmanić, "Permutations Unlabeled Beyond Sampling Unknown," *IEEE Signal Processing Letters*, vol. 26, pp. 823–827, June 2019.
- [13] M. C. Tsakiris, L. Peng, A. Conca, L. Kneip, Y. Shi, and H. Choi, "An Algebraic-Geometric Approach for Linear Regression Without Correspondences," *IEEE Transactions on Information Theory*, vol. 66, pp. 5130–5144, Aug. 2020.
- [14] M. Tsakiris and L. Peng, "Homomorphic Sensing," in *Proceedings of the 36th International Conference on Machine Learning*, pp. 6335–6344, May 2019.
- [15] D. J. Hsu, K. Shi, and X. Sun, "Linear regression without correspondence," in *Advances in Neural Information Processing Systems*, vol. 30, Curran Associates, Inc., 2017.
- [16] Ashwin Pananjady, M. J. Wainwright, and T. A. Courtade, "Linear Regression With Shuffled Data: Statistical and Computational Limits of Permutation Recovery," *IEEE Transactions on Information Theory*, vol. 64, pp. 3286–3300, May 2018.
- [17] A. Abid, A. Poon, and J. Zou, "Linear Regression with Shuffled Labels," *arXiv preprint, arXiv:1705.01342*, May 2017.
- [18] M. Slawski and E. Ben-David, "Linear regression with sparsely permuted data," *Electronic Journal of Statistics*, vol. 13, pp. 1–36, Jan. 2019.
- [19] M. Slawski, G. Diao, and E. Ben-David, "A Pseudo-Likelihood Approach to Linear Regression With Partially Shuffled Data," *Journal of Computational and Graphical Statistics*, Mar. 2021.
- [20] A. Abid and J. Zou, "A Stochastic Expectation-Maximization Approach to Shuffled Linear Regression," in *56th Annual Allerton Conference on Communication, Control, and Computing (Allerton)*, pp. 470–477, Oct. 2018.
- [21] L. Peng and M. C. Tsakiris, "Linear Regression Without Correspondences via Concave Minimization," *IEEE Signal Processing Letters*, vol. 27, pp. 1580–1584, 2020.
- [22] L. Peng, B. Wang, and M. Tsakiris, "Homomorphic Sensing: Sparsity and Noise," in *Proceedings of the 38th International Conference on Machine Learning*, pp. 8464–8475, July 2021.
- [23] G. Elhami, A. Scholefield, B. Béjar Haro, and M. Vetterli, "Unlabeled sensing: Reconstruction algorithm and theoretical guarantees," in *IEEE International Conference on Acoustics, Speech and Signal Processing (ICASSP)*, pp. 4566–4570, Mar. 2017.
- [24] Z. Wang, E. Ben-David, and M. Slawski, "Estimation in exponential family Regression based on linked data contaminated by mismatch error," *arXiv preprint, arXiv:2010.00181*, Oct. 2020.
- [25] A. A. Abbasi, A. Tasissa, and S. Aeron, "R-Local Unlabeled Sensing: A Novel Graph Matching Approach for Multiview Unlabeled Sensing Under Local Permutations," *IEEE Open Journal of Signal Processing*, vol. 2, pp. 309–317, 2021.
- [26] Y. Yao, L. Peng, and M. Tsakiris, "Unlabeled Principal Component Analysis," in *Advances in Neural Information Processing Systems*, vol. 34, pp. 30452–30464, Curran Associates, Inc., 2021.
- [27] L. Xu, J. Honda, G. Niu, and M. Sugiyama, "Uncoupled Regression from Pairwise Comparison Data," *Advances in Neural Information Processing Systems*, vol. 32, 2019.
- [28] P. Dragotti, M. Vetterli, and T. Blu, "Exact sampling results for signals with finite rate of innovation using Strang-Fix conditions and local kernels," in *IEEE International Conference on Acoustics, Speech, and Signal Processing*, vol. 4, pp. iv/233–iv/236 Vol. 4, Mar. 2005.
- [29] P. L. Dragotti, M. Vetterli, and T. Blu, "Sampling Moments and Reconstructing Signals of Finite Rate of Innovation: Shannon Meets Strang-Fix," *IEEE Transactions on Signal Processing*, vol. 55, pp. 1741–1757, May 2007.
- [30] I. Maravic and M. Vetterli, "Sampling and reconstruction of signals with finite rate of innovation in the presence of noise," *IEEE Transactions on Signal Processing*, vol. 53, pp. 2788–2805, Aug. 2005.
- [31] B. B. Haro and M. Vetterli, "Sampling Continuous-Time Sparse Signals: A Frequency-Domain Perspective," *IEEE Transactions on Signal Processing*, vol. 66, pp. 1410–1424, Mar. 2018.
- [32] L. Condat and A. Hirabayashi, "Cadzow denoising upgraded: A new projection method for the recovery of dirac pulses from noisy linear measurements," *Sampling Theory in Signal and Image Processing*, vol. 14, no. 1, pp. 17–47, 2015.
- [33] M. Simeoni, A. Besson, P. Hurley, and M. Vetterli, "CPGD: Cadzow Plug-and-Play Gradient Descent for Generalised FRI," *IEEE Transactions on Signal Processing*, vol. 69, pp. 42–57, 2021.
- [34] E. J. Candès and C. Fernandez-Granda, "Towards a mathematical theory of super-resolution," *Communications on Pure and Applied Mathematics*, vol. 67, no. 6, pp. 906–956, 2014.
- [35] G. Tang, B. N. Bhaskar, P. Shah, and B. Recht, "Compressed sensing off the grid," *IEEE Transactions on Information Theory*, vol. 59, no. 11, pp. 7465–7490, 2013.
- [36] J. Cadzow, "Signal enhancement—a composite property mapping algorithm," *IEEE Transactions on Acoustics, Speech, and Signal Processing*, vol. 36, pp. 49–62, Jan. 1988.
- [37] L. Peng, X. Song, M. C. Tsakiris, H. Choi, L. Kneip, and Y. Shi, "Algebraically-initialized Expectation Maximization for Header-free Communication," in *IEEE International Conference on Acoustics, Speech and Signal Processing (ICASSP)*, pp. 5182–5186, May 2019.

- [38] P. J. Huber and E. M. Ronchetti, *Robust Statistics*. John Wiley & Sons, Inc., 2 ed., 2009.
- [39] F. R. Hampel, E. M. Ronchetti, P. J. Rousseeuw, and W. A. Stahel, *Robust Statistics: The Approach Based on Influence Functions*. John Wiley & Sons, Inc., 2011.
- [40] V. J. Yohai, "High Breakdown-Point and High Efficiency Robust Estimates for Regression," *The Annals of Statistics*, vol. 15, pp. 642–656, June 1987.
- [41] A. M. Zoubir, V. Koivunen, E. Ollila, and M. Muma, *Robust Statistics for Signal Processing*. Cambridge: Cambridge University Press, 2018.
- [42] P. Rousseeuw and V. Yohai, "Robust Regression by Means of S-Estimators," in *Robust and Nonlinear Time Series Analysis*, pp. 256–272, Springer US, 1984.
- [43] C. H. Müller and N. Neykov, "Breakdown points of trimmed likelihood estimators and related estimators in generalized linear models," *Journal of Statistical Planning and Inference*, vol. 116, pp. 503–519, Oct. 2003.
- [44] T.-W. Chen, T. J. Wardill, Y. Sun, S. R. Pulver, S. L. Renninger, A. Baohan, E. R. Schreier, R. A. Kerr, M. B. Orger, V. Jayaraman, L. L. Looger, K. Svoboda, and D. S. Kim, "Ultra-sensitive fluorescent proteins for imaging neuronal activity," *Nature*, vol. 499, pp. 295–300, July 2013.
- [45] J. Vogelstein, A. Packer, T. Machado, T. Sippy, B. Babadi, R. Yuste, and L. Paninski, "Fast nonnegative deconvolution for spike train inference from population calcium imaging," *J Neurophysiology*, vol. 104, no. 6, pp. 3691–3704, 2010.
- [46] B. Béjar and G. Mischler, "A finite rate of innovation approach for the estimation of a stream of decaying exponentials," in *54th Asilomar Conference on Signals, Systems, and Computers*, pp. 1497–1501, Nov. 2020.
- [47] J. Oñativia, S. R. Schultz, and P. L. Dragotti, "A finite rate of innovation algorithm for fast and accurate spike detection from two-photon calcium imaging," *Journal of Neural Engineering*, vol. 10, p. 046017, Aug. 2013.
- [48] GENIE Project, Janelia Farm Campus, HHMI, "Simultaneous imaging and loose-seal cell-attached electrical recordings from neurons expressing a variety of genetically encoded calcium indicators," 2015. [Online]. Available: <http://dx.doi.org/10.6080/K02R3PMN>.

APPENDIX

A. Generalization for $M \geq 2$ channels

In this section, we extend the result from Section II to the case of more than two shuffled signals. We begin by generalizing our definition of shuffled measurement vectors for $M \geq 2$ signals.

Definition 2. Let $\mathbf{q}_{mm'} \in \{0, 1\}^N$, $m, m' \in \{1, \dots, M\}$, $M \in \mathbb{N}_{\geq 2}$ be binary variables with the property

$$\sum_{m=1}^M \mathbf{q}_{mm'} = \sum_{m'=1}^M \mathbf{q}_{mm'} = \underbrace{(1 \quad 1 \quad \dots \quad 1)}_{:=\mathbf{1}}^T. \quad (16)$$

Vectors $\mathbf{y}_1, \mathbf{y}_2, \dots, \mathbf{y}_M \in \mathbb{R}^N$ are referred to as shuffled measurement vectors of $\mathbf{x}_1, \mathbf{x}_2, \dots, \mathbf{x}_M \in \mathbb{R}^N$, if they follow the linear system

$$\underbrace{\begin{pmatrix} \mathbf{Q}_{11} & \mathbf{Q}_{12} & \dots & \mathbf{Q}_{1M} \\ \mathbf{Q}_{21} & \mathbf{Q}_{22} & \dots & \mathbf{Q}_{2M} \\ \vdots & \vdots & \ddots & \vdots \\ \mathbf{Q}_{M1} & \mathbf{Q}_{M2} & \dots & \mathbf{Q}_{MM} \end{pmatrix}}_{:=\mathbf{\Pi}_q} \underbrace{\begin{pmatrix} \mathbf{x}_1 \\ \mathbf{x}_2 \\ \vdots \\ \mathbf{x}_M \end{pmatrix}}_{:=\mathbf{x}} = \underbrace{\begin{pmatrix} \mathbf{y}_1 \\ \mathbf{y}_2 \\ \vdots \\ \mathbf{y}_M \end{pmatrix}}_{:=\mathbf{y}}. \quad (17)$$

where $\mathbf{Q}_{mm'} := \text{diag}(\mathbf{q}_{mm'})$. Note that in (17), for each index in \mathbf{y}_m exactly one sample from $\mathbf{x}_1, \dots, \mathbf{x}_M$ is selected.

Lemma 1. If a matrix $\mathbf{\Pi}_q$ follows the definition in (17) then $\mathbf{\Pi}_q$ is a permutation matrix.

Proof. (Lemma 1) Let a matrix $\mathbf{\Pi}_q$ follow the definition in (17). From (16), it follows that every row and every column of $\mathbf{\Pi}_q$ add up to 1. Since elements of $\mathbf{\Pi}_q$ can only take the values 0 or 1, the property can only hold, if exactly one element per row and column is '1' and the remaining ones are '0'. Thus, by Definition 1, $\mathbf{\Pi}_q$ is a permutation matrix. \square

Based on Definitions 2 and 1 as well as Corollary 1, we are now ready to state the following result.

Lemma 2. Let $\mathbf{y}_1, \mathbf{y}_2, \dots, \mathbf{y}_M \in \mathbb{R}^N$ be shuffled measurement vectors of some unknown noiseless sample vectors $\mathbf{x}_1, \mathbf{x}_2, \dots, \mathbf{x}_M \in \mathbb{R}^N$ and let $\mathbf{U} \in \mathbb{R}^{N \times K}$ with full column rank, i.e., $\text{rank}(\mathbf{U}) = K$. If $N \geq 2K$ and $\mathbf{x}_1, \mathbf{x}_2, \dots, \mathbf{x}_M \in \mathcal{R}(\mathbf{U})$, then $\mathbf{x}_1, \mathbf{x}_2, \dots, \mathbf{x}_M$ can be uniquely recovered from $\mathbf{y}_1, \mathbf{y}_2, \dots, \mathbf{y}_M$ and \mathbf{U} .

Proof. (Lemma 2) Let $\mathbf{y} = (\mathbf{y}_1^\top, \mathbf{y}_2^\top, \dots, \mathbf{y}_M^\top)^\top$ and $\mathbf{x} = (\mathbf{x}_1^\top, \mathbf{x}_2^\top, \dots, \mathbf{x}_M^\top)^\top$. Then, according to Definition 2, $\mathbf{y} = \mathbf{\Pi}_q \mathbf{x}$, where $\mathbf{\Pi}_q$ follows the definition in (17) and is thus an unknown permutation matrix (Lemma 1). Further, since \mathbf{U} is such that $\mathbf{x}_m \in \mathcal{R}(\mathbf{U})$, $m = 1, \dots, M$, we can express $\mathbf{y} = \mathbf{\Pi}_q \mathbf{x}$ as

$$\mathbf{y} = \underbrace{\begin{pmatrix} \mathbf{Q}_{11} & \dots & \mathbf{Q}_{M1} \\ \vdots & \ddots & \vdots \\ \mathbf{Q}_{M1} & \dots & \mathbf{Q}_{MM} \end{pmatrix}}_{:=\mathbf{\Pi}_q} \underbrace{\begin{pmatrix} \mathbf{U} & & \\ & \ddots & \\ & & \mathbf{U} \end{pmatrix}}_{:=\mathbf{A}} \underbrace{\begin{pmatrix} \beta_1 \\ \vdots \\ \beta_M \end{pmatrix}}_{:=\beta}, \quad (18)$$

where β_m are the expansion coefficients of \mathbf{x}_m in \mathbf{U} , that is, $\mathbf{x}_m = \mathbf{U}\beta_m$, $m = 1, \dots, M$. Since \mathbf{U} has full column rank, the matrix \mathbf{A} has full column rank and because $N \geq 2K$ it follows from Corollary 1 that the regression coefficients β can be uniquely recovered from (18). Hence, $\mathbf{x}_1, \mathbf{x}_2, \dots, \mathbf{x}_M$ can be uniquely recovered up to an ordering of the channels. \square

Thus, we can show in the following that Theorem 1 holds:

Proof. (Theorem 1) Since the measured signals \mathbf{y}_m , $m = 1, \dots, M$ follow Definition 2, and since samples are permuted across channels, we have that the addition of all the observed channels \mathbf{y}_m is left unaffected by the shuffling and equals the sum of the underlying \mathbf{x}_m signals:

$$\mathbf{x}_\Sigma = \sum_{m=1}^M \mathbf{x}_m = \sum_{m=1}^M \mathbf{y}_m = \mathbf{y}_\Sigma.$$

Because of (7) the resulting vector \mathbf{y}_Σ also follows a frequency domain representation of the same form:

$$Y_{\Sigma, \ell} = X_{\Sigma, \ell} = \sum_{k=0}^{K_\Sigma-1} a_{\Sigma, k} e^{-j2\pi \ell t_{\Sigma, k}},$$

$$\ell = 0, \dots, N-1, \quad t_{\Sigma, k} \in [0, 1),$$

where $\{t_{\Sigma, k}\}_{k=0}^{K_\Sigma-1} \subseteq \{t_{m, k}, k = 0, \dots, K_m - 1, m = 1, \dots, M\}$ is the subset of distinct locations of all the signals with associated amplitudes $\{a_{\Sigma, k}\}_{k=0}^{K_\Sigma-1}$. Note that the amplitudes can also be different from $a_{m, k}$, if some channels share the support. Therefore, the time-domain signal \mathbf{x}_Σ can be represented as

$$\mathbf{x}_\Sigma = \mathbf{W}\mathbf{V}_\Sigma \mathbf{a}_\Sigma \quad (19)$$

where \mathbf{V}_Σ is a Vandermonde matrix constructed from $t_{\Sigma, k}$ (i.e., $[\mathbf{V}_\Sigma]_{\ell, k} = v_k^\ell$ with $v_k = e^{-j2\pi t_{\Sigma, k}}$), and where $\mathbf{a}_\Sigma = (a_{\Sigma, 0}, a_{\Sigma, 1}, \dots, a_{\Sigma, K_\Sigma-1})^\top$. Note that the Vandermonde matrix \mathbf{V}_Σ has full column rank since the locations $t_{\Sigma, k} \in [0, 1)$ (hence the v_k) are all distinct. From the sampling theorem given in [9], it is known that, in such a case, the parameters $(\{t_{\Sigma, k}, a_{\Sigma, k}\}_{k=0}^{K_\Sigma-1})$ can be uniquely recovered from \mathbf{x}_Σ if $N \geq 2K_\Sigma$. This means that we can recover the support of the sparse signal \mathbf{x}_Σ and therefore construct the matrix \mathbf{V}_Σ . If we let $\mathbf{U} := \mathbf{W}\mathbf{V}_\Sigma$, the signals $\mathbf{x}_1, \mathbf{x}_2, \dots, \mathbf{x}_M$ can be represented as

$$\mathbf{x}_1 = \mathbf{U}\beta_1, \mathbf{x}_2 = \mathbf{U}\beta_2, \dots, \mathbf{x}_M = \mathbf{U}\beta_M, \quad (20)$$

for some coefficient vectors $\beta_1, \beta_2, \dots, \beta_M \in \mathbb{R}^{K_\Sigma}$. Since \mathbf{U} is also full rank with $\text{rank}(\mathbf{U}) = K_\Sigma$ (this follows from \mathbf{W} and \mathbf{V}_Σ being both full rank), and $N \geq 2K_\Sigma$, it follows from Lemma 2 that $\mathbf{x}_1, \mathbf{x}_2, \dots, \mathbf{x}_M$ can be uniquely recovered up to an ordering of the channels. \square